Optical conductivity of manganites: Crossover from Jahn-Teller small polaron to coherent transport in the ferromagnetic state

M. Quijada* and J. Černe
Laboratory for Physical Sciences, College Park, Maryland 20740

J. R. Simpson
Materials Research Laboratory, Department of Physics, University of Maryland, College Park, Maryland 20742

H. D. Drew
Laboratory for Physical Sciences, College Park, Maryland 20740
and Materials Research Laboratory, Department of Physics, University of Maryland, College Park, Maryland 20742

K. H. Ahn and A. J. Millis
Department of Physics and Astronomy, The Johns Hopkins University, Baltimore, Maryland 21218

R. Shreekala, R. Ramesh, M. Rajeswari, and T. Venkatesan
Materials Research Laboratory, Department of Physics, University of Maryland, College Park, Maryland 20742
(Received 16 March 1998)

We report on the optical properties of the hole-doped manganites $Nd_{0.7}Sr_{0.3}MnO_3$, $La_{0.7}Ca_{0.3}MnO_3$, and $La_{0.7}Sr_{0.3}MnO_3$. The low-energy optical conductivity in the paramagnetic-insulating state of these materials is characterized by a broad maximum near 1 eV. This feature shifts to lower energy and grows in optical oscillator strength as the temperature is lowered into the ferromagnetic state. It remains identifiable well below T_c and transforms eventually into a Drude-like response. This optical behavior and the activated transport in the paramagnetic state of these materials are consistent with a Jahn-Teller small polaron. The optical spectra and oscillator strength changes compare well with models that include both double exchange and the dynamic Jahn-Teller effect in the description of the electronic structure. [S0163-1829(98)06848-9]

I. INTRODUCTION

The discovery of colossal magnetoresistance (CMR) in hole-doped ferromagnetic manganite materials of the form $(Ln)_{1-x}(A)_xMnO_{3-\delta}$, where Ln is a lanthanide and A is an alkaline-earth element, has revived interest in this complex magnetic system.[1] These systems crystallize in a pseudocubic perovskite structure. The electronically active orbitals are the Mn d orbitals and the number of electrons per Mn is $4-x$. Hund's rule coupling implies that three electrons are localized on the t_{2g} orbitals forming a core spin of $S_c=\frac{3}{2}$, while the remaining $1-x$ electrons go into a band derived from the e_g orbitals. When the material is doped in the range of $0.2<x<0.5$, it undergoes a phase transition between a paramagnetic insulator and a ferromagnetic metal at temperature T_c.

The double-exchange model proposed by Zener[2] was the mechanism first used to explain the paramagnetic to ferromagnetic phase transformation in these conducting materials. In this model the hopping probability between Mn sites for the electrons residing on the e_g orbitals is maximal when the core spins are parallel and minimal when they are antiparallel. Hence, the model provides a qualitative explanation for the metallic conduction below T_c (spins well aligned), and insulating behavior above T_c (spins randomly aligned). However, recent theoretical as well as experimental reports suggest that, within this model, the coupling between the charge and spin is not enough to explain the high-temperature insulating phase. In particular, theoretical arguments[3–6] indicate the need to include effects that are related to the strong coupling between charge and the lattice such as the Jahn-Teller (JT) effect associated with the Mn^{3+} ions. In this picture a JT distortion lifts the degeneracy in the e_g orbitals causing a splitting into lower and upper e_g levels that is static for $0<x<0.2$ and appears to be dynamic for $x>0.2$. Since the JT distortion is associated with the Mn^{3+} ions it can localize the e_g electrons in the paramagnetic phase of the alloys leading to insulating behavior, whereas the increased e_g band width in the ferromagnetic state quenches the JT effect and produces metallic conduction. Optical absorption studies of the stoichiometric parent compound $LaMnO_3$ give evidence for static JT distortions. Analysis of the optical conductivity of $LaMnO_3$ within the local-spin-density approximation suggests that the observed gap in the optical conductivity of about 1.0 eV corresponds to the optical process of promoting a hole between the JT split e_g bands on the Mn^{3+} ions.[7,8] Optical measurements have also been reported for the series of compounds $La_{1-x}Sr_xMnO_3$.[9–11] The results from optical reflectivity studies of metallic samples ($x>0.2$) show large transfers of spectral weight from high frequencies to low frequencies as the samples are cooled from the paramagnetic state through T_c into the ferromagnetic metallic state.[9,10] In these studies it is also concluded that a simple double-exchange picture is not enough to explain the observed changes in the optical spectral weight over such a large energy scale compared to

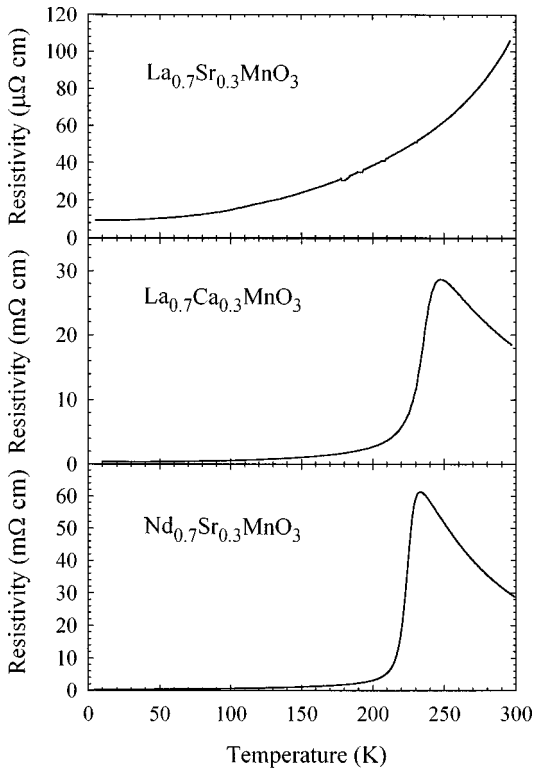

FIG. 1. Temperature dependence of the resistivity for the three samples. The metal to insulator transition is apparent for the NSMO and LCMO.

k_BT for all doping concentrations.[9,10] Other recent experimental results also suggest the presence of strong lattice effects in these materials: shifts in the IR phonon frequencies related to the Mn-O bonds in $La_{0.7}Ca_{0.3}MnO_3$ near T_c have been reported by Kim *et al.*;[12] anomalies in the local structure of the MnO_6 octahedron near T_c obtained from neutron scattering studies of $La_{1-x}Ca_xMnO_3$ have been interpreted in terms of Jahn-Teller distortion;[13] a magnetic-field-driven structural phase transformation was observed[14] in $La_{1-x}Sr_xMnO_3$, for $x=0.170$; thermopower measurements of $La_{0.7}Ca_{0.3}MnO_3$ have also suggested the presence of small polaronic behavior above T_c that is found to disappear below the insulator-metal transition.[15]

Localization of the e_g electron on the Mn^{3+} ions in the paramagnetic state of the doped manganites due to Jahn-Teller distortions is a self-trapping effect, i.e., a small polaron.[5] If the carriers are localized due to this electron-phonon coupling, there should be an optical signature of the small polaron associated with photoinduced hopping of the carriers, as has been reported in systems such as TiO_2.[16,17] In an earlier publication we reported evidence for the JT small polaron in $Nd_{0.7}Sr_{0.3}MnO_3$.[18] In this paper we present an extension of that earlier work by comparing the optical conductivity derived from transmittance and reflectance measurements of $La_{0.7}Sr_{0.3}MnO_3$, $La_{0.7}Ca_{0.3}MnO_3$, and an oxygen annealed $Nd_{0.7}Sr_{0.3}MnO_3$ thin film as a function of temperature and for photon energies up to 5 eV. As in the previous work, the optical conductivity on these new films show large shifts in spectral weight from visible to infrared frequencies as the temperature is lowered through T_c, demonstrating broadband changes in electronic properties on an energy scale several orders of magnitude larger than k_BT_c. In the paramagnetic-insulating state of all three materials the optical conductivity at low energies is characterized by a broad maximum near 1 eV as we reported earlier for $Nd_{0.7}Sr_{0.3}MnO_3$ and interpreted in terms of the photon induced hopping of the Jahn-Teller small polaron. Therefore these new experiments show that this feature is generic for the paramagnetic state of the pseudocubic manganites. This spectral feature is found to shift to lower energy and grow in optical oscillator strength as the system enters into the ferromagnetic state. It gradually transforms into a Drude-like response well below T_c where the transport is metallic. Nevertheless, the polaron peak can still be identified at temperatures substantially below T_c.

At higher frequencies, the spectrum of $\sigma_1(\omega)$ indicates the presence of a temperature dependent optical absorption feature centered at 3 eV and a large spectral feature at 4 eV which still has a weak temperature dependence. The 3-eV feature appears to be more prominent in the paramagnetic state as is seen by looking at the difference in conductivity: $\Delta\sigma_1=\sigma_1(T)-\sigma_1(10\text{ K})$. The energy position of this feature suggests that it involves transitions between the Hund's rule spin-split e_g derived bands. The 4 eV feature is most likely related to a similar feature that is seen in the undoped materials where it has been identified as a charge transfer transition between the O_{2p} and the Mn_d derived bands.[11]

We also present an analysis of the magnitude and temperature dependence of the spectral weight $\int d\omega\sigma_1(\omega)$ and of its relation to the spin wave stiffness at $T=0$.[3] This analysis extends and corrects an earlier treatment by including the finite Hund's rule splitting and a more realistic treatment of the e_g bands.[3–6]

II. EXPERIMENT

A. Sample characterization

The samples used in this study were thin films of $Nd_{0.7}Sr_{0.3}MnO_3$, $La_{0.7}Sr_{0.3}MnO_3$, and $La_{0.7}Ca_{0.3}MnO_3$ grown on $LaAlO_3$ substrates by pulsed laser deposition in an N_2O atmosphere[19] (in what follows we will refer to these samples as NSMO, LSMO, and LCMO, respectively). The films are epitaxial as revealed by x-ray diffraction, and show 3 MeV He^+ ion Rutherford backscattering channeling spectra with a minimum yield of 3.8%, indicating a high degree of crystallinity. Additional characterization of these samples was done by performing resistivity and ferromagnetic resonance measurements.[20,21]

Figure 1 shows the temperature dependence of the resistivity for the three samples that we studied using standard four-probe measurements. The temperature at which the resistivity peaks, T_p, is 235 K for NSMO, 250 K for LCMO, and 360 K for LSMO. These values are close to the Curie temperature T_c in these samples. In addition to the observed progression in T_c, there is also a variation in the low-temperature value of the resistivity ρ. The values for ρ at $T=10$ K are 350 $\mu\Omega$ cm for NSMO, 300 $\mu\Omega$ cm for LCMO, and 10 $\mu\Omega$ cm for the LSMO sample. To the best of our knowledge, these are the lowest values for the resistivities ever reported for these materials indicative of the high quality of these thin-film samples. The observed low-temperature resistivities correspond to conductivities greater than

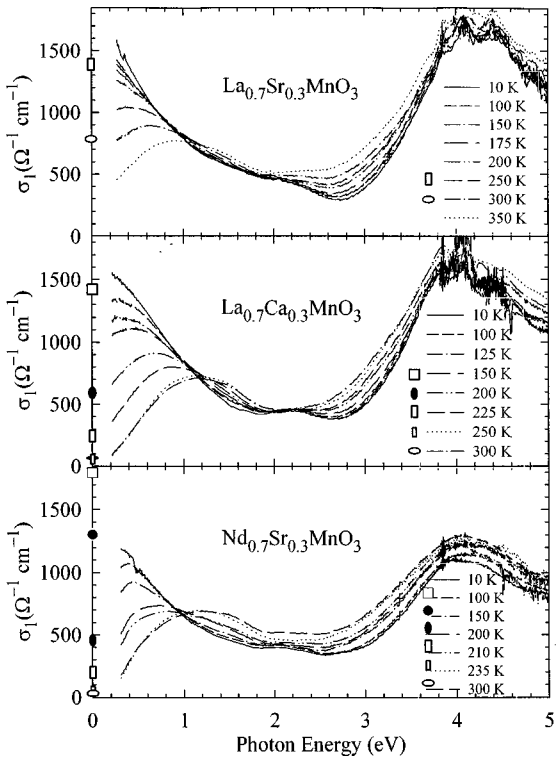

FIG. 2. Frequency dependence of the real part of the optical conductivity σ_1 for the three samples at different temperatures.

the Mott minimum conductivity ($\sigma_{\mathrm{Mott}}=0.656(e^2/h)n^{1/3} \approx 500\ \Omega^{-1}\ \mathrm{cm}^{-1}$ if the carrier density is determined by the divalent alkaline earth substitution x/Ω_0, where Ω_0 is the unit cell volume). It is noteworthy that the low-temperature resistivities previously reported in the literature for bulk and film samples generally correspond to conductivities below the Mott minimum conductivity, which suggests that those samples were not homogeneous. Our results imply that previous reports do not reflect intrinsic behavior, perhaps because of sample inhomogeneity. We suggest that proposals of superunitary scattering[22,23] be reexamined as the intrinsic behavior becomes better determined.

B. Optical techniques

Transmittance and reflectance measurements were performed using a Fourier transform spectrometer (BOMEM DA3) to cover the investigated regions of 5–25 meV and 0.20–5 eV. These are the frequency ranges for which the $LaAlO_3$ substrate is transparent. Measurements in this wide range of frequencies were accomplished by using different combinations of sources, beamsplitters and detectors. The uncertainty in the absolute transmittance obtained from the reproducibility in the different spectral ranges is $\pm 2\%$. Likewise, the uncertainty in the absolute reflectance spectra is estimated at $\pm 3\%$. Temperature-dependent measurements were made possible by mounting the samples on the cold finger of a continuous flow cryostat with room-temperature windows for optical access. The cryostat unit was placed inside the sample compartment of the spectrometer. The temperature of the sample was stabilized by using a temperature controller with a calibrated Si diode sensor mounted near the sample and a heating element attached to the cold finger of the cryostat.

At far infrared frequencies the real part of the optical conductivity σ_1 is determined from the observed transmittance given by

$$\frac{T_{\mathrm{FS}}}{T_S}=[(1+Z\sigma_1)^2+(Z\sigma_2)^2]^{-1}, \tag{2.1}$$

in the thin-film limit $d/\delta \ll 1$, which is well satisfied in our samples (here $\delta=\lambda/4\pi\kappa$, is the skin depth and d is the film thickness). T_{FS} and T_S are the transmittance of the film/substrate and substrate respectively, $Z=Z_0 d/n+1$, where Z_0 is the free space impedance, and n the refractive index of the substrate. Inverting Eq. (2.1) we can write

$$\sigma_1=Z^{-1}\left[\sqrt{\frac{T_S}{T_{\mathrm{FS}}}-(Z\sigma_2)^2}-1\right] \leqslant Z^{-1}\left[\sqrt{\frac{T_S}{T_{\mathrm{FS}}}}-1\right]. \tag{2.2}$$

The final inequality becomes an equality when $\sigma_2/\sigma_1 \ll 1$. Terahertz measurements on a LSMO sample[24] confirm that $\sigma_2/\sigma_1 \ll 1$ is a valid approximation in the regime of interest, $0<\omega<100\ \mathrm{cm}^{-1}$.

At higher frequencies, the optical properties of the samples in the infrared-UV range are derived from the measured transmittance and reflectance by numerically inverting the Fresnel formulas for a thin film on a weakly absorbing thick substrate. The interference (etalon) effects from the substrate are averaged by using low spectral resolution in the measurement and by averaging over the interference fringes in the analysis.[25] This procedure yields the index of refraction and extinction coefficient of the thin-film material, n_f and κ_f, respectively, using n and κ for the substrate. The results of n_f and κ_f are then used to derive the other optical constants such as the dielectric function, $\epsilon(\omega)$, or the optical conductivity $\sigma(\omega)$.[26] Since this technique does not rely on Kramers-Kronig analysis it permits reliable measurement of the optical conductivity up to the high-frequency cutoff of the optical equipment (5 eV).

This analysis assumes that the index of refraction n and κ of the substrate are known quantities. In all of the substrate samples that we measured, we found the index to be roughly constant, $n \simeq 2.0$, and sample independent in the 0.2–5 eV range.[27] Although the values for the extinction coefficient were small in this same range $10^{-3}-10^{-4}$, we found some variation in κ for different samples of $LaAlO_3$, especially near the cutoff frequency 0.2 eV. The differences are sufficiently large that it is necessary to use the values for n and κ for the substrate on which the film was grown in the analysis since the effect of κ in the substrate is similar to the effect of σ_1 in the sample ($\sim 10\%$). Therefore, after the film was measured, it was removed from the substrate and the transmittance and reflectance of the bare substrate were measured. This procedure ensured that the proper values of n and κ for the substrate were used in the final inversion of the data.

III. RESULTS: OPTICAL SPECTRA

The optical conductivity in the far infrared was estimated as described in Sec. II B. Because of the narrow range of the transmission window of the $LaAlO_3$ substrates and the featureless transmissivity from 20 to 100 cm^{-1} these data provide only a low-frequency data point to our broadband con-

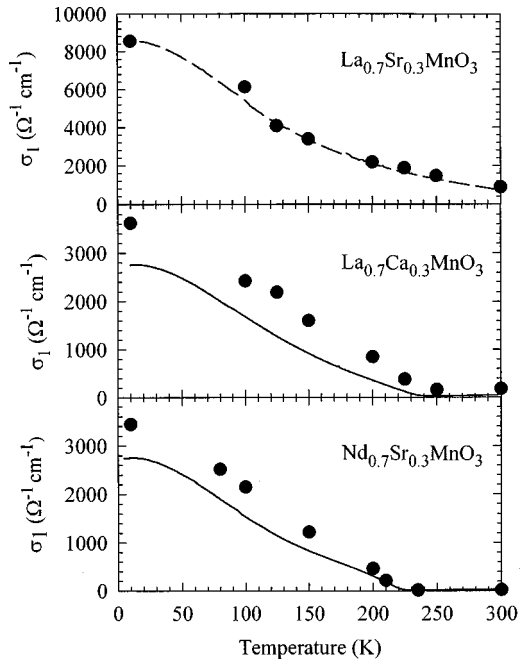

FIG. 3. Comparison of the temperature dependence of the dc (solid lines) and ac (circles) conductivities at 20 cm^{-1} derived from Eq. (2.2). The dc conductivity for the $La_{0.7}Sr_{0.3}MnO_3$ sample (the dashed curve) has been divided by 10 in order to fit the data in the same scale.

ductivity spectra shown in Fig. 2. It is interesting to compare this far-infrared conductivity with the dc conductivity of the same films. Figure 3 displays a comparison of the measured dc conductivity and the derived conductivities at 20 cm^{-1} using Eq. (2.2). We noticed a reasonable agreement between the ac and dc values for LCMO and NSMO samples. However, a striking disagreement is found for the LSMO sample. The measured dc conductivity in this sample is roughly 10 times larger than the ac values obtained at 20 cm^{-1}. Similar results have been observed in another high conductivity LSMO film. However, typical LSMO films have a resistivity of around 100 $\mu\Omega$ cm in better agreement with the ac values. The observed discrepancy for the high conductivity films is particularly significant when it is recalled that the far-infrared ac conductivity derived from Eq. (2.2) is an upper limit of the true value. Therefore, the discrepancy is not a consequence of granularity in the film since this effect would lead to an effective dc resistivity larger than the intrinsic value due to the higher resistivity of the grain boundaries. We believe that the observed behavior may be explained in terms of an anisotropic conductivity arising from strain effects in the films. Such effects may be expected in materials with a strong coupling between the electrons and the lattice as we are reporting in this paper. Further studies of these effects are in progress.

The results of the real part of the optical conductivity $\sigma_1(\omega)$ for the three samples measured at different temperatures are shown in Fig. 2. The symbols near zero frequency are obtained from the far-infrared transmittance measurements as described above. The IR conductivity is seen to extrapolate reasonably to the far-infrared value except for a downturn near the low-frequency IR cutoff. This effect is believed to be related to the difficulties in characterizing the differences in the extinction coefficient of the substrates near the IR cutoff as discussed earlier. Therefore we do not trust the data below approximately 0.3 eV. In the results shown in Fig. 2 we find that, near and above T_c, the optical conductivity for the three samples is dominated by a broad maximum near 1 eV with a peak value of roughly 600–700 Ω^{-1} cm^{-1}, only slightly higher than the Mott conductivity. We also notice that the feature near 1 eV evolves in temperature in very much the same way for the different alloys. These data indicate that this feature is universal in the hole doped pseudocubic manganites. In all the samples, the broad maximum in the conductivity spectrum above T_c shifts lower in frequency and grows in oscillator strength as temperature is decreased through T_c as can be seen in Fig. 2. The peak structure remains identifiable well below T_c, but as the temperature is lowered further into the metallic range the low-frequency part fills in and eventually $\sigma_1(\omega)$ increases with decreasing frequency for $T \ll T_c$. This indicates a Drude response and coherent conduction at low temperatures and low frequencies in all of the samples. The results for the new oxygen annealed $Nd_{0.7}Sr_{0.3}MnO_3$ sample differ from the results on an unannealed sample, reported previously, which did not show a Drude-like response even at the lowest temperature, although the $T > T_c$ behavior was similar to that observed here. The earlier sample had a lower T_c and a much higher dc resistivity ($\sigma_{dc} < \sigma_{Mott}$) than the present sample even at the lowest T and similar to values generally reported in the literature on NSMO. Clearly, the different oxygen treatment of the two samples produced different behaviors in their dc transport and optical properties.

Throughout the infrared the reflectance and transmittance of the films is dominated by σ_1 and is relatively insensitive to ϵ_1. Therefore our results for ϵ_1 are less reliable. Nevertheless, we find that ϵ_1 remains positive down to at least 0.5 eV despite the apparent free-carrier response of $\sigma_1(\omega)$ at low temperature, which would be expected to produce a negative ϵ_1 characteristic of a metal. The observed behavior is not completely unexpected since interband transitions between the two e_g bands are expected in this spectral range. Nevertheless, this behavior indicates that the spectral weight of the coherent component of the conductivity is only a small fraction of the total spectral weight in all of these samples.

The other major spectral feature in the optical data is the strong peak in the conductivity near 4 eV. The noisy appearance of the conductivity data near the peak of this feature is a consequence of the very small transmittance of the films due to the strong absorption at the peak. Also, this feature appears noticeably weaker in $Nd_{0.7}Sr_{0.3}MnO_3$.

IV. DISCUSSION

A. Overview

In this section we discuss in more detail several of the striking features of the optical conductivity data shown in Fig. 2. There are three main peaks: at ~1, 3, and 4 eV. A qualitative picture of the states and optical transitions is shown in Fig. 4. The important orbitals are the Mn e_g and O_{2p} levels. Optical absorption is controlled by the electric dipole matrix element and allowed transitions involve motion of a charge either from one Mn site to another or from

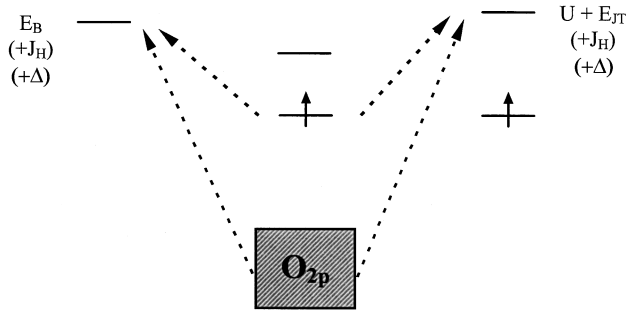

FIG. 4. States and energies involved in optical transitions. The central portion shows initial states left and right panels show allowed optical transitions and final-state energies referenced to the Fermi energy. The initial states in the central panel are: a filled oxygen p band and a Mn site with one e_g electron. The twofold degeneracy of the e_g levels is assumed split by a local Jahn-Teller distortion. The level splitting (not indicated on the figure) is E_{JT}. The right-hand portion indicates the optical transition in which the charge is moved from an O or Mn site to a Mn site that is already singly occupied. The final state energy is the sum of the Jahn-Teller splitting E_{JT}, the e_g-e_g Coulomb repulsion U, the charge transfer energy D (if the electron came from an O site) and the Hund's energy J_H (if the transferred electron has spin antiparallel to the core spin). The left-hand portion indicates an optical transition to a Mn that initially has no e_g electrons. In this case the e_g levels are degenerate and the final-state energy is shifted by the breathing distortion energy E_B (and Δ and J_H, if appropriate).

an O to a Mn. Reference 28 argues that transitions from one e_g orbital to another one *on the same site* appear in the optical spectrum, but we believe these transitions have negligible oscillator strength because both the initial and the final states have d symmetry with respect to the same origin.

There are several important energies. One is the e_g-O_{2p} charge-transfer energy Δ. Another is the Jahn-Teller energy E_{JT}: if a Mn site has one e_g electron then a local even-parity lattice distortion that breaks cubic symmetry may occur; this splits the e_g levels by an amount E_{JT}. A third is the breathing distortion energy E_B: at a Mn site with no e_g electrons a symmetric ''breathing'' distortion of the surrounding oxygens may occur: if (as occurs in an optical transition) an e_g electron is added on a time scale that is fast compared to a phonon frequency (so the lattice does not have time to relax) the final state is shifted up in energy by E_B. In LCMO with $x=0.5$, the low temperature phase is charge ordered and both breathing and Jahn-Teller distortions occur.[29] The amplitudes of these distortions are approximately equal, suggesting $E_B \sim E_{\mathrm{JT}}$. A fourth energy is the ''Hubbard U'' repulsion[30] between two e_g electrons on the same site. As will be discussed below, available evidence suggests that the effective U describing the low- ($\omega<4$ eV) energy physics of the e_g band is weak. A final energy is the Hund's coupling J_H: each Mn has a $S=\frac{3}{2}t_{2g}$ core spin (not shown in Fig. 4); any e_g electrons may have spin parallel or antiparallel to the core spin; the ''antiparallel'' state is higher by an energy J_H.

In the remainder of this section we shall argue that the 1-eV feature involves e_g-e_g transitions within the parallel spin manifold; the 3-eV feature is due to e_g-e_g transitions in which the final state is antiparallel and the 4 eV feature is the e_g-O_{2p} transition.

The most striking feature of the data in this energy range is the broad peak centered at $\omega \approx 1$ eV ($\sim$1.3 eV in the LCMO and NSMO samples, and perhaps at a somewhat lower energy in LSMO), which is evident in the paramagnetic phase in all samples and that, as T is decreased below the magnetic T_c, loses intensity and shifts to lower frequency, eventually evolving into the Drude-like response observed at very low temperatures. This feature was first observed by Okimoto *et al.*[9] and was interpreted by them as the ''parallel'' to ''antiparallel'' transition, implying a $J_H \sim 1.5$ eV. However, as noted by Millis, Muellar, and Shraiman the temperature dependence of the spectral weight of the 1-eV feature is inconsistent with this interpretation. Because the electric dipole matrix element preserves spin, the antiparallel final state is inaccessible if the material is in the fully polarized ferromagnetic ground state, so the oscillator strength in the antiparallel transition should decrease as T is lowered below T_c. However, as seen in Figs. 2 and 5, the intensity in the peak feature grows as T is decreased below T_c, even as the feature broadens and shifts to lower energies, inconsistent with the antiparallel interpretation. We, therefore, believe it involves parallel spin e_g-e_g transitions only. However, the temperature dependence of $\sigma(\omega)$ near $\omega=3$ eV is consistent with transitions to an e_g antiparallel final state. As can clearly be seen in Fig. 5, which displays the difference $[\sigma_1(\omega,T)-\sigma(\omega,T=10\ \mathrm{K})]$, a peak at $\omega \approx 3$ eV grows in strength as the temperature is raised and the core spins are disordered.

Returning now to the 1 eV feature, we ascribe it to e_g-e_g transitions. As will be discussed in detail in the next section, the oscillator strength is consistent with that expected for dipole allowed d-d charge-transfer transitions between Mn ions on different sites. The insulating nature of the paramagnetic phase and the peaklike shape of the absorption suggests that it arises from excitation of carriers out of bound states. One possibility is localization due to disorder, as suggested by Ref. 31. We think this is unlikely because of the universal appearance of the feature in manganites of widely varying dc conductivities.[7,9,10] As noted by Jung *et al.*,[28] the characteristic energy of the absorption feature in the paramagnetic state of the doped materials is similar to that observed in insulating $LaMnO_3$, where a $\sim$1.5 eV gap appears in the e_g manifold due to the presence of a long-range ordered Jahn-Teller distortion. In $LaMnO_3$ this feature is believed to be due to the e_g-e_g transition shown in the right-hand panel of Fig. 4; the gap of 1.5 eV corresponds to a band-center to band-center energy difference of about 2.5 eV and we identify this energy as $E_{\mathrm{JT}}+U$ for $LaMnO_3$.

Doped materials in the paramagnetic phase were predicted[3] to have lattice distortions similar to those occurring in $LaMnO_3$ (but without the long-range order) and these distortions (with amplitude approximately 70% of those in $LaMnO_3$) have recently been directly observed in neutron pair-distribution-function[13] and extended x-ray-absorption fine-structure (EXAFS[32]) experiments. We, therefore, interpret the 1-eV feature observed at $T>T_c$ in our doped samples as being due to the excitation of a carrier out of a bound state produced by a strong local lattice distortion (and into a final state also modified by the lattice distortions). Of course, in doped materials the e_g electron concentration is less than one per site, so transitions such as those shown in

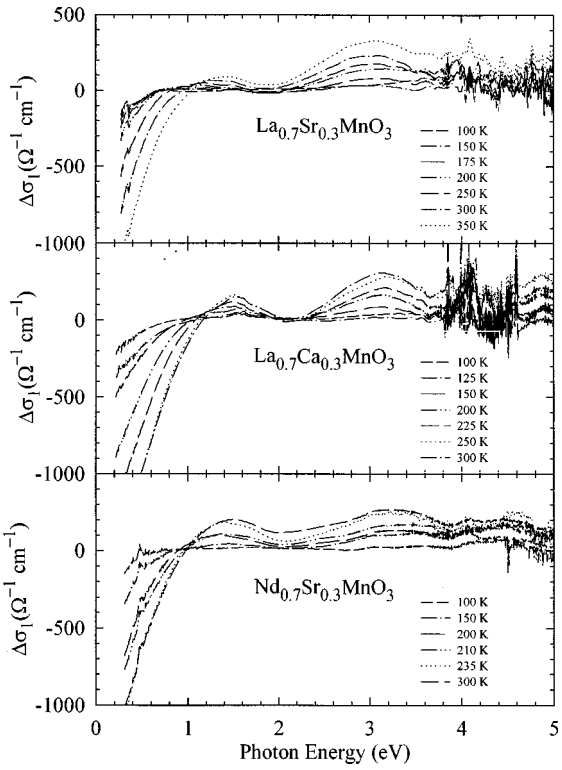

FIG. 5. Difference in optical conductivity $\Delta\sigma_1=\sigma_1(T)-\sigma_1(10K)$ for the three samples. Notice the feature at 3.0 eV that shows up more prominently in the paramagnetic state.

the left panel of Fig. 4 are also possible. The fact that only one (broad) feature is observed suggests that the energy shift due to the breathing distortion, E_B, is comparable to the Jahn-Teller plus Coulomb energy $E_{\rm JT}+U$.

As the temperature is decreased below T_c, the 1-eV feature grows in intensity and broadens, and eventually evolves into the Drude-like response observed at very low temperatures. This behavior corresponds to the collapse of the Jahn-Teller small polaron as the system goes into the ferromagnetic state. It can be understood in terms of a model proposed by Millis, Mueller, and Shraiman[3] that incorporates double exchange and dynamic JT effects in the system. In this model, the behavior of the system is controlled by the dimensionless effective coupling constant λ defined as

$$\lambda=\frac{E_{JT}}{t\langle\cos(\theta_{ij}/2)\rangle}, \tag{4.1}$$

where t is the hopping probability, and θ_{ij} is the relative angle between neighboring spins. The temperature dependence is controlled by the $\langle\cos(\theta_{ij}/2)\rangle$ factor, which goes from $\frac{2}{3}$ in the paramagnetic state to 1 in the ferromagnetic state. Within this model a qualitative description of the data shown in Fig. 2 is as follows: In the paramagnetic state λ is larger than λ_c, the critical value for the formation of a small polaron. The 1-eV feature corresponds to the photoionization of the small polaron at $\hbar\omega=E_B+\frac{1}{2}E_{\rm JT}$ (see Fig. 4). As the temperature is decreased, the spins become aligned and λ decreases becoming smaller than λ_c leading to a collapse of the JT small polaron and coherent Drude-like conduction at low temperatures. The optical conductivity calculated within this model show shifts in oscillator strength and linewidth as function of λ that compare well to the experimental results shown in Fig. 2 below 2 eV.[5] The behavior of the resistivities, the Curie temperatures and the optical properties of these materials indicate that LSMO, LCMO, and NSMO have a progressively increasing JT coupling λ. We emphasize that in all the samples the JT small polaron feature remains for intermediate temperatures below T_c. This is consistent with thermopower and EXAFS measurements that also suggest evidence for small polaronic behavior in the LCMO near T_c.[15,32] The downward shift in the polaron feature and the onset of metallic conductivity indicate a gradual transition from a small polaron to a large polaron and a corresponding gradual growth of the strength of the coherent conductivity.

Another aspect of the data shown in Fig. 2 is a large redistribution of spectral weight from optical transitions occurring above 2 eV to below the 1-eV feature discussed above. The temperature dependence of $\sigma_1(\omega)$ is seen to extend up to the upper limit of our measurements (5 eV). In the range from 2 eV to 5 eV the conductivity is dominated by the strong absorption at $\omega\simeq 4.0$ eV. The assignment of the optical process involved in this transition is made by comparing it with the result of the undoped parent compound $LaMnO_3$. In this material, a similar peak in the optical conductivity has been observed at this frequency and assigned to a charge-transfer transition between the O_{2p} and the e_g derived bands.[7,11] The T dependence of the 4-eV feature does not, however, account for the missing spectral weight when the sample is warmed above T_c as can be seen in Fig. 5. To fully account for all the low-frequency oscillator strength in the ferromagnetic state it is clear that it will be necessary to include contributions up to and beyond the 5-eV limit of our measurements. The temperature dependence of the spectral weight will be discussed further in the next section.

B. Comparison to theory: Magnitude and temperature dependence of optical spectral weight

This section presents a more quantitative comparison of data to theory. The main results are as follows: (i) The e_g electron kinetic energy is largest (and effective electron-phonon interaction weakest) in LSMO, while the kinetic energy is smallest (and electron-phonon interaction strongest) in NSMO, with LCMO being intermediate. (ii) In all compounds at lowest temperature the e_g kinetic energy is of the order of the band theory value, suggesting that at this temperature the effects of the electron-phonon and electron-electron interaction are relatively weak. (iii) The change in e_g kinetic energy between the lowest temperature and T_c is too large to be consistent with models involving only double exchange, but is consistent with theories based on the interplay of double exchange and electron-phonon coupling. (iv) There is a reasonable consistency between the optical estimates of the electron kinetic energy and the observed low temperature spin wave stiffness (our analysis here generalizes and corrects statements made in Ref. 3). (v) The magnitude of the change in optical absorption near $\omega\approx 3$ eV is quantitatively consistent with the interpretation, given in the previous section, of the 3-eV peak as transitions to the antiparallel final state.

Because calculations of $\sigma(\omega,T)$ including both a realistic treatment of the e_g band structure and the effects of the electron-phonon interaction are not available, we focus the discussion on the spectral weight $S(\omega)$ defined by

$$S(\omega)=\frac{2}{\pi}\int_0^{\omega} d\omega\sigma_1(\omega). \tag{4.2}$$

It is sometimes convenient to define an effective number of electrons per unit cell $N_{\rm eff}(\omega)$ and a kinetic energy $K(\omega)$ via

$$N_{\rm eff}(\omega)=\frac{V_{\rm cell}m}{e^2}S(\omega), \tag{4.3}$$

$$K(\omega)=\frac{a_0}{e^2}S(\omega), \tag{4.4}$$

where $V_{\rm cell}$ is the unit cell volume and $a_0=V_{\rm cell}^{1/3}$. If the integral in Eq. (4.2) is carried out to $\omega=\infty$ the familiar *f*-sum rule implies one obtains $N_{\rm eff}(\omega=\infty)=N$, the total number, core plus valence, of electrons in the unit cell. $S(\omega<\infty)$ gives a partial sum rule that may give information about low-lying states of interest. For the manganites the low-lying states of interest are the e_g electrons; in the analysis that follows we will first present some theoretical results, then determine an ω such that $S(\omega)$ is a good estimate of the spectral weight in the e_g-e_g transitions and finally use the magnitude and temperature dependence of the determined spectral weight to infer the results listed above.

We begin with theory. We assume the physics of interest is determined by carriers hopping between Mn e_g-symmetry *d* levels on sites of a simple cubic lattice of lattice constant a_0 and interacting with each other, with the lattice, and with core spins of magnitude $S_c=\frac{3}{2}$. The Hamiltonian is

$$\hat{H}=-\tfrac{1}{2}\sum_{\substack{i\boldsymbol{\delta}\\ ab}} t_{\boldsymbol{\delta}}^{ab}[e^{i\mathbf{A}\cdot\boldsymbol{\delta}}d_{ia\alpha}^{\dagger}d_{i+\boldsymbol{\delta}b\alpha}+\text{H.c.}]$$

$$-J_H\sum_{\substack{ia\\ \alpha\beta}}\mathbf{S}_{ci}\cdot d_{ia\alpha}^{\dagger}\boldsymbol{\sigma}_{\alpha\beta}d_{ia\beta}+H_{\rm INT}. \tag{4.5}$$

Here $d_{ia\alpha}^{\dagger}$ creates an electron with spin α in e_g orbital *a* on site *i*, J_H is the Hund's coupling between the itinerant electrons and the core spins, $H_{\rm INT}$ represents the other interactions, and $t_{\boldsymbol{\delta}}^{ab}=t_{\boldsymbol{\delta}}^{ba}$ represents the direction-dependent amplitude for an electron to hop from orbital *b* to orbital *a* on site $i+\boldsymbol{\delta}$. $\mathbf{A}$ is the vector potential and conductivity is calculated by linear response in $\mathbf{A}$ as usual. The calculated band structure[33,34] is in fact well fit by a $t_{\boldsymbol{\delta}}^{ab}$, which involves only nearest-neighbor hopping that is only nonzero for one particular linear combination of orbitals, and has the magnitude $t_0\simeq 0.6$ eV. The particular linear combination depends on the basis chosen for the e_g doublet and on the direction of $\boldsymbol{\delta}$. If basis states $|\mathbf{x}^2-\mathbf{y}^2\rangle$ and $|3\mathbf{z}^2-r^2\rangle$ are chosen then for $\boldsymbol{\delta}=\hat{z}$ the only nonzero element of *t* is the one between $|3\mathbf{z}^2-r^2\rangle$ orbitals on the two sites. The analysis that follows does not depend in any important way on the form chosen for $t_{\boldsymbol{\delta}}^{ab}$, but the numbers of course do. In this model the quantity $K=K(\omega=\infty)$ defined in Eq. (4.4) is given by

$$K=\frac{1}{6N_{sites}}\sum_{\substack{i\boldsymbol{\delta}\\ ab}} t_{\boldsymbol{\delta}}^{ab}\langle d_{ia\alpha}^{\dagger}d_{i+\delta b\alpha}+\text{H.c.}\rangle. \tag{4.6}$$

Here $\langle\rangle$ stands for a quantum and thermal expectation value in the ensemble of eigenstates of $\hat{H}$. Note that because $\hat{H}$ involves only a subset of all orbitals (in the present case, only the e_g-symmetry *d* levels) the total optical oscillator strength in transitions described by $\hat{H}$ is less than the full *f*-sum rule value Ne^2/m and indeed is given by the expectation value of an operator (in the present case, the kinetic energy). This expectation value may depend on temperature and interaction strength. The missing *f*-sum rule oscillator strength comes from transitions between e_g orbitals and other orbitals not described by $\hat{H}$; these transitions will have oscillator strengths that also depends on temperature and interaction. We are not aware of theoretical results indicating which transitions are most important in restoring the spectral weight. Interestingly, the data in Fig. 5 suggest that in the manganites the e_g-O_{2p} transitions are not the ones primarily responsible for restoring the spectral weight. If $H_{\rm INT}=0$, the noninteracting value K_0 may be evaluated at $T=0$. For $x=0.3$ we find

$$K_0=0.46t_0\cong 0.28\ \text{eV}. \tag{4.7}$$

$K_0=0.28$ eV implies the effective carrier density $N_{\rm eff}=0.54$.

If $H_{\rm INT}=0$ and a fully polarized ferromagnetic state is assumed for the core spins then the free energy is given by extremizing the kinetic energy, which is the operator whose expectation value yields *K*. Spin disorder or inclusion of $H_{\rm INT}$ will therefore change the wave function to one that does not optimize the kinetic energy. K_0 is thus an upper bound to the optical spectral weight of the model specified by Eq. (4.5) and would be a reasonable estimate for the low-*T* oscillator strength in the manganite e_g bands if interaction effects were not important. Some caution is required because the Mn-Mn hopping amplitude is a very sensitive function of the length and degree of buckling of the Mn-O-Mn bond, so the value $t_0=0.6$ eV obtained by fitting band calculations for ideal materials may not be exactly correct for the variously doped materials that have slightly different unit-cell sizes and crystal structure.

In order to compare the observed oscillator strength to the band theory estimate, we must identify the e_g contribution to the absorption. In the previous section the peak at $\omega\approx 4$ eV was identified as coming from Mn-O transitions. From the $T=10$ K curves in Fig. 2 one sees that in the LSMO and LCMO samples the Mn-O transition dominates the absorption for $\omega>2.7$ eV. For the NSMO sample the Mn-O transition is not so clearly separated. For all three samples we estimate the e_g kinetic energy at $T=0$ by integrating the data up to $\omega=2.7$ eV (see Fig. 6); this yields the values for $K(2.7)$ shown in Table I. The trend in kinetic energies is reasonable. Within the double-exchange and the Jahn-Teller pictures these kinetic energy trends predict the corresponding T_c in these materials. LSMO has the highest T_c and is the most metallic, consistent with its relatively large optically determined kinetic energy, while NSMO has the lowest T_c and is the least metallic, and also has the smallest kinetic

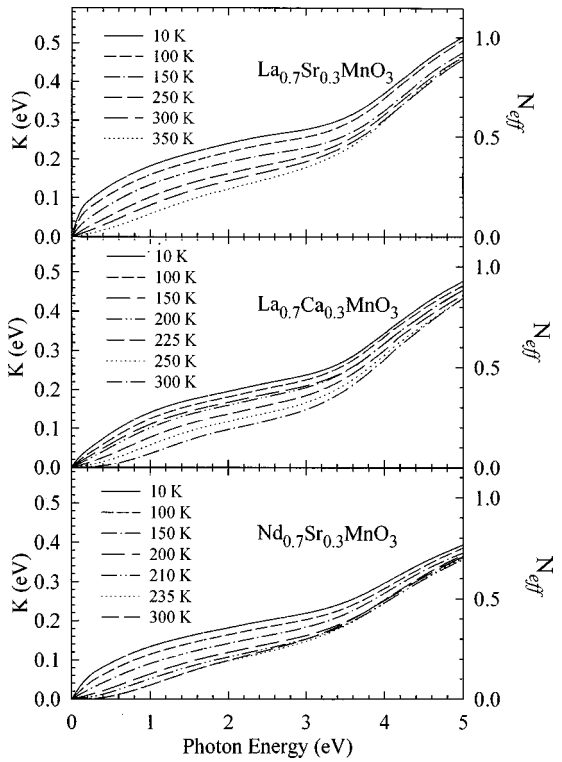

FIG. 6. Integral of the real part of the optical conductivity $\sigma_1(\omega)$ as a function of photon energy. The results are expressed in terms of kinetic energy and the carrier density N_{eff}/f.u.

energy. All of the observed kinetic energies are less than those estimated from band theory; the Ca and Nd/Sr particulary so. The discrepancy could be due to an incorrect identification of the e_g contributions to σ. However, our analysis of the temperature dependence of the spectral weight, which will be discussed below, leads us to believe that we have correctly identified the e_g transitions, and that in $La_{1-x}Ca_xMnO_3$ and $Nd_{1-x}Sr_xMnO_3$ the kinetic energy is simply less than the band prediction. However, in view of the uncertainties involved we regard the correspondence between the data and band theory as reasonable. The analysis suggests that at low T any renormalizations of the kinetic energy due to electron-electron and electron-phonon interactions are not very large.

We now consider the temperature dependence of the spectral weight, which is obviously large and provides further information regarding the relevant energy scales. As the temperature is raised from zero the core spins cease to be perfectly aligned, causing the kinetic energy to decrease. As explained in Ref. 4 the decrease in bare electron kinetic energy increases the effective electron-phonon coupling, causing a further decrease in the e_g kinetic energy. Additionally, the core spin disorder means that optical transitions in which an e_g electron goes from parallel to the core spin on one site to antiparallel to the core spin on another becomes possible. The final-state energy in this antiparallel transition is $\approx J_H S_C$. In the $J_H \rightarrow \infty$ limit the antiparallel transitions may be neglected; in the actual materials $J_H S_C$ is large enough that the parallel and antiparallel absorptions are well separated in energy and may be discussed separately. At $T=0$, the core spins are fully aligned and only parallel transitions are possible; as T is increased the spectral weight in the

TABLE I. Observed kinetic energies (in meV) and some kinetic energy ratios for the three samples, obtained by integrating the observed conductivities and using Eqs. (4.3) and (4.4). $K(2.7) \equiv K_{T=0}(\omega=2.7\text{ eV})$ is obtained by integrating the observed conductivity at lowest temperature up to 2.7 eV; $K_{\text{par}} \equiv K_{T>T_c}$ $(\omega=2.7\text{ eV})$, the spectral weight associated with parallel spin transitions, is obtained by integrating the observed conductivity at the highest temperature up to 2.7 eV. K_{anti}, the conductivity associated with the antiparallel transitions, is obtained by integrating the difference in conductivity between highest and lowest temperatures from 2.2 to 4 eV.

	LSMO	LCMO	NSMO
$K(2.7)$	260	220	200
K_{anti}	34	31	30
K_{par}	125	100	100
$\frac{K_{\text{anti}}}{K_{\text{par}}}$	0.27	0.31	0.30
$\frac{K_{\text{par}}}{K(2.7)}$	0.48	0.45	0.50

parallel spin transitions decreases both because the total kinetic energy decreases and because some of the remaining spectral weight is transferred to the antiparallel transitions. A detailed theoretical analysis of the temperature dependence of the spectral weight including finite J_H and realistic band structure is not yet available, but results for $J_H=\infty$ and a simplified band structure are given in Ref. 5. For finite J_H and more realistic band-structure statements can be made about the changes in spectral weights from $T=0$ to $T>T_c$, where the core spins may reasonably be expected to be completely uncorrelated from site to site. Calculations using the noninteracting model, Eq. (4.5) with $H_{\text{INT}}=0$, show that if the parallel and antiparallel absorptions are well separated in energy then as the temperature is raised from $T=0$ to $T>T_c$, the change in spectral weight in the parallel spin transitions is given to good accuracy by the results of the $J_H=\infty$ limit, while at $T>T_c$ the ratio of antiparallel to parallel spectral weights is approximately $2t_0/1.4J_H S_c \approx \frac{1}{3}$ (using $t_0=0.6$ eV and $J_H S_c \approx 3$ eV, which is estimated as the difference between the energies of the parallel and antiparallel absorption bands). We believe that these conclusions, which have been verified in the noninteracting limit, apply also to interacting models. We therefore analyze the $T>T_c$ data by comparing the parallel spin spectral weight to the $J_H=\infty$ calculations and the antiparallel weight to $\frac{1}{3}$ the parallel weight. The parallel-spin spectral weight is most conveniently addressed by considering the change in oscillator strength between lowest T and $T>T_c$. In double exchange only models such as Eq. (4.5) with $H_{\text{INT}}=0$, the oscillator strength decreases by $\frac{1}{3}$, i.e., $\Delta K = K(T=0) - K_{\text{par}}(T>T_c) = \frac{1}{3}K(T=0)$. Models involving the interplay of double-exchange and electron-phonon coupling can produce a larger $\Delta K/K(T=0)$ because of a feedback effect: decreasing K_{par} by increasing spin disorder increases the effective electron-phonon coupling which decreases K_{par} still further. In Ref. 5 weak, intermediate, and strong electron-phonon couplings were distinguished. The intermediate coupling regime was argued to be relevant to CMR; in this regime the phonon

renormalization of the kinetic energy is small at low T (where the behavior is metallic) but significant at high T (where the interaction has localized the electrons). This leads to $\Delta K \cong \frac{1}{2}K(T=0)$.

Table I presents the measured values of $K_{\rm par}(T>T_c)$, obtained by integrating the observed conductivity up to 2.7 eV. These values lead to $\Delta K \approx \frac{1}{2}K(T=0)$, in good agreement with theory. Further, the observed magnitude of ΔK supports the correctness of our estimate for $K(T=0)$; different estimates of $K(T=0)$ would lead to different estimates of $\Delta K/K$, in disagreement with theory.

Now we turn to the antiparallel absorption. Taking the 3-eV feature in Fig. 5 to be the antiparallel transition and integrating the difference in conductivity between the highest and lowest temperatures from 2.2 to 4 eV we find spectral weights $K_{\rm anti}$ given in Table I for the three compounds. The parallel spectral weights $K_{\rm par}$ also shown in Table I are obtained as before by integrating up to 2.7 eV. This leads to ratios of the antiparallel to the parallel spin absorptions of approximately $\frac{1}{3}$, in reasonable accord with the theoretical estimates.

We finally turn to the spin-wave dispersion that at small q has the form $\omega_{\rm magnon}=Dq^2$. The value of D is of interest because in double-exchange materials the spin stiffness is related to the amplitude for conduction electrons to hop from one site to the next, and as we have seen this is given by the conduction-band optical spectral weight. One therefore expects a relation between the optical spectral weight and the spin wave stiffness. To derive this relation ship more precisely, we consider the energy cost $\Delta E(q)$ of imposing a static distortion of wave vector q. The long-wavelength limit of this energy cost is related to the spin wave stiffness by factors involving the quantum-mechanical spin dynamics. For double exchange materials the relationship is[3]

$$D=\frac{1}{S^*}\frac{d^2}{dq^2}\,\Delta E(q)\big|_{q=0}. \tag{4.8}$$

Here $S^*=S_c+\frac{1}{2}(1-x)\cong 1.85$ is the magnetic moment per site. To calculate $\Delta E(q)$ we suppose that on each site the core spin S_c^i is characterized by polar angles (θ_i,ϕ_i) and that θ_i is small, so we are near the fully polarized $\theta_i\equiv 0$ state. On each site we rotate the e_g electron basis so that it is parallel to $\mathbf{S}_{ci}$. The rotation matrix that does this is $R_i=\cos(\theta_i/2)\hat{1}+i\,\sin(\theta_i/2)\mathbf{n}\cdot\boldsymbol{\sigma}$ where $\mathbf{n}=(n_x,n_y)$ with $n_x=\cos\phi_i$ and $n_y=\sin\phi_i$. We now calculate $E(\theta_i)-E(\theta=0)$ by second-order perturbation theory. The perturbation Hamiltonian is

$$\hat{H}_p=+\tfrac{1}{2}\sum_{\substack{i\delta\\ ab\\ \alpha\beta\gamma}} t_{\boldsymbol{\delta}}^{ab}[(\hat{1}-R^{\dagger}_{i\,\gamma\alpha}R_{i+\delta\,\gamma\beta})d^{\dagger}_{ia\alpha}d_{i+\delta b\alpha}+\text{H.c.}]. \tag{4.9}$$

Now $(1-R_i^{\dagger}R_{i+\delta})$ has a term of order θ, with which we do second-order perturbation theory, and a term of order θ^2, with which we do first-order perturbation theory. For first-order perturbation theory we take the ground-state expectation value of $\hat{H}_p$, obtaining $(\mathbf{m}_i=\theta_i\mathbf{n})$

$$E_1=\frac{K}{16}\sum_{i\delta}(m_i-m_{i+\delta})^2 \tag{4.10}$$

(note the term in $\hat{1}-R^{\dagger}R$ proportional to σ_z vanishes by symmetry). Now turn to second-order perturbation theory (neglected in some previous work[3]). The second-order perturbing Hamiltonian is

$$\hat{H}_p'=-\frac{i}{2}\sum_{\substack{i\delta\\ ab\\ \alpha\beta}} t_{\boldsymbol{\delta}}^{ab}[(\mathbf{m}_i-\mathbf{m}_{i+\delta})\cdot\boldsymbol{\sigma}](d^{\dagger}_{ia\alpha}d_{i+\delta b\alpha}-\text{H.c.}). \tag{4.11}$$

This is basically the current operator convolved with the gradient of the magnetization. In the limit $J_H\to 0$, the up and down e_g bands become equally populated and for long-wavelength spin fluctuations $\hat{H}_p'$ becomes identical to the current operator; as $q\to 0$ the second-order perturbation contribution cancels the first-order one just as do the paramagnetic and diamagnetic parts of the optical conductivity and the stiffness vanishes. In the limit $J_H\to\infty$ the contribution from $\hat{H}_p'$ vanishes. We have calculated the order q^2 term in the magnon dispersion to order $1/J_H$ using Eq. (4.5) with $H_{\rm INT}=0$ and find

$$D=\frac{Ka_0^2}{4S^*}\left[1-\frac{\alpha t^2}{J_H S_c K}\right], \tag{4.12}$$

with $\alpha=1.04$. A similar result was obtained by Furukawa[35] using a simpler electron dispersion and the dynamical mean field method. We expect a very similar result for general interacting models, but with a possibly different value of α.

The band structure estimates $t=0.6$ eV and $K=0.28$ eV, along with the experimental value $J_H S_C=2$ eV gives $D=0.16$ eV Å^2. Use of the observed K along with appropriately rescaled $t(t/t_{\rm band}=K_{\rm observed}/K_{\rm band})$ gives $D=0.18$ eV Å^2 for NSMO and LCMO and $D=0.17$ eV Å^2 for LSMO. The very weak dependence on K occurs because near $K=0.5$ the variation in first and second terms in Eq. (4.12) almost exactly cancels.

Our estimates for D are in excellent agreement with the experimental values of $D=0.19$ eV Å^2 for LSMO (Ref. 36) and 0.17 eV Å^2 for both LCMO (Ref. 37) and NSMO.[38] Also, the weak material dependence predicted by the theory is consistent with the experimental finding. However, this close agreement may be somewhat fortuitous since the parameters are not accurately known and the second order correction to D in Eq. (4.12) is not very small compared with the first-order term. Nevertheless, these results suggest that other effects that may be expected to affect the spin wave stiffness may not be significant. One such effect proposed by Solovyev, Hamada, and Terakura[8] is that in addition to the double-exchange ferromagnetic coupling there is a weaker antiferromagnetic coupling between the core spins. This would act to weaken the spin stiffness, and according to the calculations of Ref. 8 its magnitude depends sensitively on the buckling of the Mn-O-Mn bond. Also, the electron-phonon coupling might affect the second term in Eq. (4.12). Therefore the issue warrants further investigation.

V. CONCLUSIONS

We have measured and analyzed the optical conductivity of several manganite materials. We have identified the physical origin of the various features in the absorption spectrum and determined their variation with temperature and material. The temperature dependence of the spectral weight agrees quantitatively with theory and provides evidence in favor of the importance of the electron-phonon coupling. Also, the qualitative variation of T_c with the spectral weight of the different materials is consistent with the theory. The kinetic energy of the e_g electrons is found to be 10–20 % larger than predicted by band theory; in view of the uncertainties in both calculation and measurement we believe this constitutes good agreement. The relation between the optical spectral weight and the spin wave stiffness was examined. Excellent agreement was found.

ACKNOWLEDGMENTS

We would like to thank S. M. Bhagat and S. E. Lofland for performing the ferromagnetic resonance measurements on the samples prior to the optical measurements, and C. Kwon and C. Xiong for providing some of the samples. We also thank A. G. Markelz at NIST for performing the terahertz measurements. This work was supported in part by NSF-MRSEC Grant Nos. DMR-96-32521, DMR-9705482, and NIST Grant No. 70NANB5H0086.

*Present address: Code 551, Goddard Space Flight Center, Greenbelt, MD 20771.

[1] R. M. Kusters, J. Singleton, D. A. Keen, R. Mcgreevy, and W. Hayes, Physica B **155**, 362 (1989); R. Von Helmholt, J. Wecker, B. Holzapfel, L. Schultz, and K. Samwer, Phys. Rev. Lett. **71**, 2331 (1993); K. I. Chahara, T. Ohno, M. Kasai, and Y. Kozono, Appl. Phys. Lett. **63**, 1990 (1993); S. Jin, T. H. Tiefel, M. McCormack, R. A. Fastnacht, R. Ramesh, and L. H. Chen, Science **264**, 413 (1994); M. McCormack, S. Jin, T. H. Tiefel, R. M. Fleming, J. M. Phillips, and R. Ramesh, Appl. Phys. Lett. **64**, 3407 (1994); H. L. Ju, C. Kwon, Q. Li, R. L. Greene, and T. Venkatesan, *ibid.* **65**, 2109 (1994).

[2] C. Zener, Phys. Rev. B **82**, 403 (1951); P. W. Anderson and H. Hasegawa, Phys. Rev. **100**, 675 (1955); P.-G. de Gennes, *ibid.* **118**, 141 (1960).

[3] A. J. Millis, P. B. Littlewood, and Boris I. Shraiman, Phys. Rev. Lett. **74**, 5144 (1995).

[4] A. J. Millis, R. Mueller, and Boris I. Shraiman, Phys. Rev. Lett. **77**, 175 (1996).

[5] A. J. Millis, R. Mueller, and Boris I. Shraiman, Phys. Rev. B **54**, 5405 (1996).

[6] H. Roder, Jun Zang, and A. R. Bishop, Phys. Rev. Lett. **76**, 1356 (1996).

[7] J. H. Jung, K. H. Kim, D. J. Eom, T. W. Noh, E. J. Choi, Jaejun Yu, Y. S. Kwon, and Y. Chung (unpublished).

[8] I. Solovyev, N. Hamada, and K. Terakura, Phys. Rev. B **53**, 7158 (1996).

[9] Y. Okimoto, T. Katsufuji, T. Ishikawa, T. Arima, and Y. Tokura, Phys. Rev. B **55**, 4206 (1997).

[10] Y. Okimoto, T. Katsufuji, T. Ishikawa, A. Urushibara, T. Arima, and Y. Tokura, Phys. Rev. Lett. **75**, 109 (1995).

[11] T. Arima, Y. Tokura, and J. B. Torrance, Phys. Rev. B **48**, 17 006 (1993).

[12] K. H. Kim, J. Y. Gu, E. J. Choi, G. W. Park, and T. W. Noh, Phys. Rev. Lett. **77**, 1877 (1996).

[13] S. J. L. Billinge, R. G. Difrancesco, G. H. Kwei, J. J. Neumeier, and J. D. Thompson, Phys. Rev. Lett. **77**, 715 (1996).

[14] A. Asamitsu, Y. Moritomo, Y. Tomioka, T. Arima, and Y. Tokura, Nature (London) **373**, 407 (1995).

[15] M. Jaime, M. B. Salamon, K. Pettit, M. Rubinstein, R. E. Treece, J. S. Horwitz, and D. B. Chrisey, Appl. Phys. Lett. **68**, 1576 (1996).

[16] G. D. Mahan, *Many-particle Physics* (Plenum Press, New York, 1981), Chap. 6.

[17] David Emin, Phys. Rev. B **48**, 13 691 (1993).

[18] S. Kaplan, M. Quijada, H. D. Drew, D. B. Tanner, G. C. Xiong, R. Ramesh, C. Kwon, and T. Venkatesan, Phys. Rev. Lett. **77**, 2081 (1996).

[19] G. C. Xiong, Q. Li, H. L. Ju, S. N. Mao, L. Senapati, X. X. Xi, R. L. Greene, and T. Venkatesan, Appl. Phys. Lett. **66**, 1427 (1995).

[20] S. E. Lofland, S. M. Bhagat, H. L. G. C. Xiong, T. Venkatesan, R. L. Greene, and S. Tyagi, J. Appl. Phys. **79**, 5166 (1996).

[21] S. Lofland and S. Bhagat (private communication).

[22] J. M. D. Coey, M. Viret, L. Ranno, and K. Ounadjela, Phys. Rev. Lett. **75**, 3910 (1995).

[23] T. V. Ramakrishnan (private communication).

[24] A. G. Markelz (private communication).

[25] O. S. Heavens, *Optical Properties of Thin Solid Films* (Dover, New York, 1991), Chap. 4.

[26] F. Wooten, *Optical Properties of Solids* (Academic, New York, 1972), Chap. 6.

[27] Z. M. Zhang, B. I. Choi, M. I. Flik, and A. C. Anderson, J. Opt. Soc. Am. B **11**, 2252 (1994).

[28] J. H. Jung, K. H. Kim, T. W. Noh, E. J. Choi, and Jaejun Yu, Phys. Rev. B **57**, 1 (1998).

[29] P. G. Radaelli, D. E. Cox, M. Marecio, and S.-W. Cheong, Phys. Rev. B **55**, 3015 (1997).

[30] A. Chainani, M. Mathew, and D. D. Sarma, Phys. Rev. B **47**, 15 397 (1993).

[31] L. Sheng, D. Y. Xing, D. N. Sheng, and C. S. Ting, Phys. Rev. Lett. **79**, 1714 (1997).

[32] C. H. Booth, F. Bridges, G. H. Kwei, J. M. Lawrence, A. T. Carnelia, and J. J. Neumeier, Phys. Rev. Lett. **80**, 853 (1998).

[33] W. E. Pickett and D. Singh, Phys. Rev. B **53**, 1146 (1996).

[34] L. F. Matheiss (unpublished).

[35] N. Furukawa, J. Phys. Soc. Jpn. **65**, 1174 (1996).

[36] M. C. Martin, G. Shirane, Y. Endoh, K. Hirota, Y. Moritomo, and Y. Tokura, Phys. Rev. B **53**, 14 285 (1996).

[37] J. W. Lynn, R. W. Erwin, J. A. Borchers, Q. Huang, A. Santoro, J-L. Peng, and Z. Y. Li, Phys. Rev. Lett. **76**, 4046 (1996).

[38] J. A. Fernandez-Baca, P. Dai, H. Y. Huang, S-W. Cheong, and C. Kloc, Phys. Rev. Lett. **80**, 4012 (1998).